ChemComm

COMMUNICATION

View Article Online
View Journal | View Issue

Cite this: *Chem. Commun.*, 2017, 53, 4834

Received 28th March 2017,
Accepted 5th April 2017

DOI: 10.1039/c7cc02354e

rsc.li/chemcomm

Insights into the surface chemistry and electronic properties of sp^2 and sp^3-hybridized nanocarbon materials for catalysis†

Yangming Lin,[abc] Zhenbao Feng,[d] Linhui Yu,[e] Qinging Gu,[ac] Shuchang Wu[c] and Dang Sheng Su*[af]

Ultra-dispersed nanodiamond and its derivatives (UNDDs), including bucky nanodiamond and onion-like carbon, offer superior catalytic behavior relative to other nanocarbons. However, a systematic study of their unique properties has been rarely achieved. Their surface chemistry and electronic properties are therefore studied to reveal the essential differences of UNDDs compared to other nanocarbons for catalysis.

Nanocarbon catalysis has been considered as a potential candidate to meet the goals of sustainable and green chemistry over the past few years.[1] Numerous achievements have demonstrated that carbon materials, such as nitrogen-doped activated carbon, reduced porous graphene oxide and nitrogen-doped carbon nanotube arrays, exhibit excellent catalytic activity as compared to some industrial transition-metal based or noble-based catalysts in the liquid phase, in the gas phase, as well as in electrochemical reactions.[2] Unlike these sp^2-hybridized carbon materials, sp^3-hybridized ultra-dispersed nanodiamond (ND) and its derivatives (UNDDs), including sp^3/sp^2-hybridized bucky nanodiamond (BND) and sp^2-hybridized onion-like carbon (OLC), have emerged as a new category of the nanocarbon family.[3] ND has abundant surface oxygen species including carboxylic acids, ketones, phenols, lactones and so on.[4] BND consists of a sp^3 carbon core covered with a few sp^2 graphite-like shell layers that can be directly synthesized by the graphitization of ND in an inert atmosphere or under vacuum ($T < 1500$ °C, Fig. S1, ESI†). It not only benefits from the remarkable surface properties of graphene-based nanomaterials but also combines the intrinsic characters of a diamond core. Upon increasing the annealing temperature ($T \geq 1500$ °C, Fig. S1, ESI†), BND will further phase transfer into OLC, which is a fascinating non-planar-related material with multiple sp^2 curved closed concentric graphite-like shells.

As new members in the carbonous family, UNDDs possess interesting physicochemical properties, such as superior thermal and chemical stability, high surface energy and unique electronic structure. These properties have made UNDDs competitive candidates for catalytic reactions beside conventional metal-based catalysts.[5] Moreover, some recent achievements have highlighted that UNDDs exhibit superior catalytic behavior in comparison to other sp^2-hybridized nanocarbon materials (*e.g.*, nanographite, nanotubes, activated carbon, graphene) for some important catalytic reactions, such as ethylbenzene dehydrogenation and phenolic oxidation.[6–8] It should be pointed out that the essential differences between a UNDD system and conventional sp^2-hybridized nanocarbons in catalytic reactions have rarely been studied, and the origin of the catalytic behavior remains elusive and controversial. As such, it is therefore highly desirable to clarify the structure–property relationship in more detail in an effort to elucidate their underlying catalytic applications. In this work, we compare the surface chemistry and electronic structures of representative sp^2- and sp^3-hybridized nanocarbon materials by using XPS, temperature programmed desorption (TPD) and ultraviolet photoelectron spectroscopy (UPS), and attempt to give insights into the distinct physicochemical properties of UNDDs and other nanocarbons. Moreover, two probe reactions (nitrobenzene reduction and selective oxidation of 2,3,6-trimethylphenol) are used to reveal the direct correlation between the electronic structure and the catalytic activity.

By using electron energy loss spectroscopy (EELS), the surface electronic structure and graphitization transformation of UNDDs were firstly studied. As shown in Fig. 1a, the main peaks located at about 292 eV in the carbon K-edge of UNDDs correspond to the characteristic 1s → σ* transitions and the shoulder peaks at 285 eV, which are assigned to the 1s → π* transition, indicate the

[a] *Shenyang National Laboratory for Materials Science, Institute of Metal Research, Chinese Academy of Sciences, Shenyang, 110016, P. R. China*
[b] *School of Chemistry and Materials Science, University of Science and Technology of China, Hefei, 230001, P. R. China*
[c] *Max Planck Institute for Chemical Energy Conversion, Stiftstrasse 34–36, Mülheim an der Ruhr, 45470, Germany*
[d] *School of Physics Science and Information Engineering, Liaocheng University, Hunan Road 1, Liaocheng 252000, P. R. China*
[e] *State Key Laboratory of Photocatalysis on Energy and Environment, Research Institute of Photocatalysis, Fuzhou University, Fuzhou 350002, P. R. China*
[f] *Department of Inorganic Chemistry, Fritz Haber Institute of the Max Planck Society, Faradayweg 4-6, Berlin, 14195, Germany. E-mail: dangsheng@fhi-berlin.mpg.de*
† Electronic supplementary information (ESI) available. See DOI: 10.1039/c7cc02354e

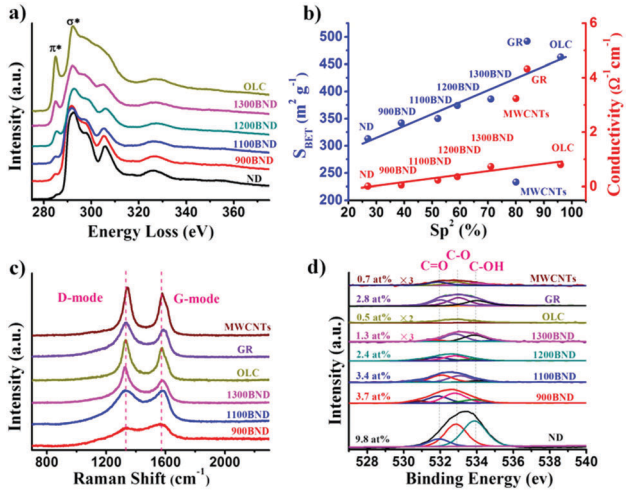

Fig. 1 (a) Electron energy loss spectroscopy (EELS) spectra of UNDDs. (b) Relationship among the relative fraction of sp^2 carbon, the specific surface area, and conductivity. (c) Raman spectra of representative carbon materials measured using a 532 nm laser. (d) XPS O1s spectra of representative carbon materials. The O1s spectra are divided by fitting the peak maximum within ±0.1 eV and applying a full width at half-maximum (FWHM) of 1.4–1.6 eV. The value of the mixed Gaussian–Lorentzian is maintained at 40%.

presence of surface sp^2 carbon.[9] Upon increasing the annealing temperature, a decrease in the 1s → σ* intensity and a gradual increase in the 1s → π* intensity are observed, which show the effective conversion from sp^3 to sp^2 carbon. Moreover, the fraction of sp^2 carbon readily calculated by EELS (with highly oriented pyrolytic graphite (HOPG) as the reference material) is shown in Fig. 1b. The content of sp^2 carbon of ND is about 27%. This indicates that the surface of ND may involve an amorphous core–shell structure that is composed of mixed sp^2/sp^3 bonding of carbon atoms.[6b,10] When the synthetic temperature reaches 1500 °C, the corresponding sp^2 content of OLC is 96%, suggesting that the phase transformation from sp^3 to sp^2 carbon is almost complete. In addition, the fraction of sp^2 carbon of representative graphene (GR) and multi-walled carbon nanotubes (MWCNTs) is around 84% and 80%, respectively. The sp^2 graphitization degree of OLC is much higher than that of GR and MWCNTs. With respect to specific surface area, there is a good linear relationship among ND, BND and OLC. The specific surface area of UNDDs increases from 313 $m^2\ g^{-1}$ for ND to around 460 $m^2\ g^{-1}$ for OLC. A similar linear tendency can be found in the electrical conductivity of the UNDDs. With the increase of the sp^2 carbon content, the electrical conductivity of UNDDs increases from 0.011 $\Omega^{-1}\ cm^{-1}$ for ND (insulator) to 0.802 $\Omega^{-1}\ cm^{-1}$ for OLC (conductor), but the value is still lower than that of GR (4.3 $\Omega^{-1}\ cm^{-1}$) and MWCNTs (3.2 $\Omega^{-1}\ cm^{-1}$).

Raman spectroscopy was used to study the surface structures of the samples. As displayed in Fig. 1c, the D-bands (~1325 cm^{-1}) of BND and OLC significantly enhanced with increasing synthesis temperature from 900 °C to 1500 °C, which is attributed to the phase transformation of sp^2/sp^3 hybridized BND to sp^2-hybridized OLC. Interestingly, the G-bands shift from 1593 cm^{-1} for BND to 1574 cm^{-1} for OLC, analogous to GR and MWCNTs. This result indicates that the surface carbon structures of OLC should consist of ordered graphite-like layers. In contrast, ND and BND are composed of highly defective graphite-like shell layers. This is evidenced by the results of HRTEM (Fig. S2, ESI†). The surface of purified ND is covered with amorphous and disordered carbon (Fig. S2a, ESI†). The identified interlayer spacing of 0.340 nm in the outer shell and the lattice spacing of 0.206 nm in the core can be assigned to the (002) plane of graphite and the (111) plane of diamond, respectively.[5c] Depending on the calcination temperature, the number of graphite-like shells of BND increases from a few layers for 900BND to multiple curved concentric graphite-like shell layers of OLC (Fig. S2d, ESI†). The particle sizes of all the ND, BND and OLC samples are about 5–8 nm. The highly defective graphite-like layers of ND and BND may be in favor of the *in situ* formation of active sites during reactions. Here, due to the non-sensitivity of ND (insulator) to a 532 nm laser, we do not find any obvious peaks in the Raman spectra. As displayed in Fig. 1d, the XPS O1s spectra of carbon materials can be deconvoluted into three peaks corresponding to an unsaturated carbonyl group (C═O, ~531.8 eV), an ester-like or anhydride group (C–O, ~532.9 eV) and a phenolic group (C–OH, ~534.0 eV). By comparing the oxygen species of various carbon materials, it was found that ND has the highest amount of oxygen species (9.8 at%), signifying that ND may provide a potential active platform for catalytic reactions due to its abundant surface chemistry information. The oxygen contents of OLC (0.5 at%) and 1200BND (2.4 at%) are close to those of typical MWCNTs (0.7 at%) and GR (2.8 at%), but the oxygen species of the OLC only involve C–O groups.

The surface group evolution of ND to OLC during the annealing process is a dynamic process. Temperature programmed desorption (TPD) is used to investigate this dynamic behavior. Upon increasing the temperature to 700 °C, some representative oxygen functional groups, such as carboxyl (–COOH, ~450 °C), anhydride (O═C–O–C═O, ~550 °C), ethers (C–O–C, ~650 °C) and phenol (C–OH, ~700 °C), will be effectively removed, leading to the release of both CO and CO_2 gases (Fig. 2a and b). When the annealing temperature is above 800 °C, the surface C═O is the only existing oxygen group in theory. The obvious signals of CO and CO_2 of ND represent the richer surface chemistry properties as compared with other carbon materials. Actually, the gradual detachment of functional oxygen groups causes the formation of dangling bonds on carbon atoms, which can reconstruct and combine to form π-bonds, indicating that the onset temperature of graphitization (namely, phase transformation) approximates to 800–900 °C. The HRTEM result of the 900BND sample further

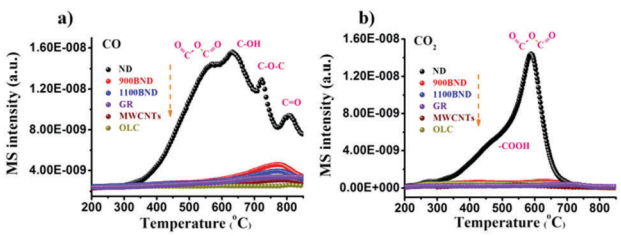

Fig. 2 TPD profiles of various carbon materials in helium at a heating rate of 10 K min^{-1}, (a) CO, m/z = 28; (b) CO_2, m/z = 44.

supports this speculation (Fig. S2b, ESI†). The reconstructive phase transformation generates sp^2-hybridized carbon shells on the outside of the ND, followed by continuous graphitization to the inside of the particle upon increasing the temperature.[11] Structural defects of the ND surface, inherent or derived from the detachment of surface functional groups, increase the reactivity of the surface carbon atoms, which greatly facilitates the phase transformation process.[12] As the temperature exceeds 1300 °C, the initially highly disordered graphite-like shells become increasingly more graphitic with a lower defect density. A fully transformed highly ordered OLC could be obtained when the temperature is above 1500 °C (Fig. S2d, ESI†). Compared with ND, GR and MWCNTs do not exhibit the competitive signals of CO and CO_2 that can be ascribed to the lower concentration of oxygen groups and the highly ordered graphite structure.

The thermostability and oxidation resistance of UNDDs have been demonstrated to play important roles in gas-phase catalysis. In other previous studies, Barnard and colleague applied a calculated model based on the extrapolated atomic heat of formation, and proposed that the thermostability of BND was better than that of ND.[13] Gogotsi *et al.* studied the standard enthalpies of formation at 25 °C over various nanostructured carbons, assuming that the thermostability followed the order graphite > BND > ND > SWCNTs > OLC. The high stability of BND may be attributed to the oxygen-containing functional groups bonded to the sp^2 structure.[14] In the present work, we found that OLC exhibited better thermostability and oxidation resistance compared to other carbon materials, measured using thermogravimetric analysis (TG) under different atmospheres (Fig. S3, ESI†). Although the content of oxygen species among some carbon materials is similar, the weight losses of GR (7.8%) and MWCNTs (4.2%) are higher than those of BND (1.3–3.4%) and OLC (1.0%), but lower than that of ND (13.8%) under an argon atmosphere. Additionally, the oxidation onset temperature of OLC is up to 600 °C, suggesting its feasibility in catalysis under a high-oxidation atmosphere. ND, with the highest concentration of oxygen species, exhibits a similar oxidation resistance to 900BND and 1100BND. The observed behavior may be correlated to their specific core–shell surface.

An ultraviolet photoelectron spectroscopy (UPS) source can excite only valence band electrons and thus it can provide information about the distribution of electrons in the valence band, work function and density of states (DOS) near the Fermi level. As shown in Fig. 3a, the valance band spectra of the carbon materials exhibit three kinds of characteristic peaks located at about 3.0, 7.0 and 8.5 eV, which can be assigned to the C2p–π, π–σ and σ electrons, respectively.[15] Using HOPG as a reference, there is no obvious difference in the binding energy of π (~3.0 eV) and σ (~7.5 eV) in the cases of BND and OLC, but the π and σ bands of multi-walled carbon nanotubes (MWCNTs) and graphene (GR) are found to shift to higher binding energies (3.8 eV and 8.5 eV). Moreover, at the region near the Fermi level (Fig. 3b), BND and OLC show a steeper increase in DOS as compared to MWCNTs and GR. These results suggest that the BND with lower π and σ electronic binding energies and enhanced DOS may be more beneficial to be activated than those of MWCNTs and GR under the same conditions. Compared with ND, the BND samples show an increase in intensity at ~3.0 eV, which is suggestive of an increase in the graphitic sp^2 carbon content (Fig. 1a and b). It should be noted that the binding energy of σ of ND (~8.2 eV) is also lower than those of MWCNTs and GR. Here, the signal of the σ band derives from the surface disordered carbon of ND rather than the bulk sp^3 carbon that is deactivated under UPS because of its own insulating properties. These results suggest that UNDDs may be activated at a lower energy cost than those of MWCNTs and GR under identical conditions, that is, UNDDs may have a higher surface energy. This fact well matches the theoretical prediction.[16]

The work function (Φ) is the minimum energy needed for inner electrons to escape from their nuclei, that is, a lower work function implies that the electrons of the samples have a lower excitation energy barrier.[17] As displayed in Fig. 4, regardless of ND, BND and OLC catalysts exhibit lower work function values than those of MWCNTs and GR. In general, the surface groups and electronic structures of the samples are two of the main factors that affect the work function.[18] It is noteworthy that compared with GR (2.8 at%) and MWCNTs (0.7 at%), 1200 BND and OLC with similar oxygen contents (2.4 and 0.5 at%, respectively) have lower work functions. Moreover, the result of the fitting curve of BND indicates that the content of sp^2 carbon is not the key factor that affects the work functions of GR, MWCNTs and BND. All these facts demonstrate that the lower work function of BND compared with those of MWCNTs

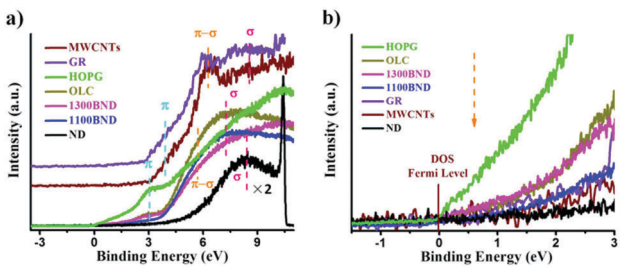

Fig. 3 (a) Valance band spectra of various carbon materials. (b) A magnified region near the Fermi level of carbon materials.

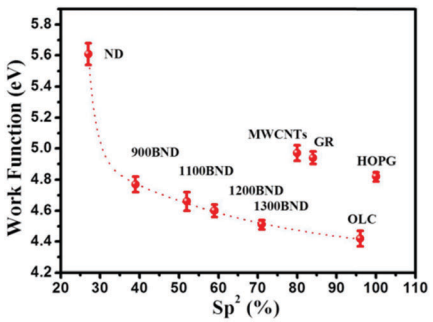

Fig. 4 Relationship between the fraction of sp^2 carbon and the work function over different carbon materials. Work functions were determined from the secondary electron cutoff of UPS He I spectra using nickel metal as a reference.

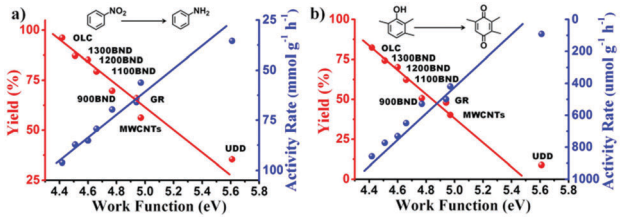

Fig. 5 The dependence of the work function on the catalytic activity over different carbon materials for the reduction of nitrobenzene (a) and the selective oxidation of 2,3,6-trimethylphenol (b). Reaction conditions: (a) 25 mg catalyst, 10 mmol nitrobenzene, 6 equiv. N_2H_4, 100 °C, 4 h. (b) 8 mg catalyst, 0.1 mmol 2,3,6-trimethylphenol, 70 °C, 12 h, 3.6 equiv. *t*-butylhydroperoxide (TBHP), 5 mL trifluorotoluene (TFT).

and BND could be explained in terms of the destabilization of the π-electrons (lower π electronic binding energy of UNDDs) rather than surface groups or the content of sp^2 carbon.[19] Such specific π-electrons may be attributed to the curvature of the graphitic shell. A similar result on the effect of the curvature on the work function in the case of carbon nanotubes has been previously reported.[20] The difference in work function among UNDDs may be assigned to surface groups or graphitization degrees. It is therefore reasonable to expect that the specific electronic structures (π and σ) of UNDDs as compared to other carbon materials are energetically favorable to activate electrons originating from the valence band of the catalyst under low energy conditions, and to have a higher surface energy, and hence may lead to the facile formation of activated complexes for some potential catalytic reactions.

To verify the potential relationship between the electronic structure and the catalytic activity, the reduction of nitrobenzene and the selective oxidation of 2,3,6-trimethylphenol as probe reactions are tested. As shown in Fig. 5, OLC with the lowest work function exhibits the best catalytic activity (96.4% and 82.3%, respectively). Moreover, directly proportional relationships between the work function and yield or activity rate are observed over different carbon materials towards the two reactions, indicating that electronic properties have a positive effect on the catalytic performance.

In summary, the essential differences between UNDDs and some typical sp^2-hybridized carbon materials (*e.g.* GR and MWCNTs) in surface chemistry and electronic properties have been investigated in detail. The observed abundant oxygen species and the surface highly defective graphite-like shells of ND and BND may be favorable to adsorb reactants and the formation of active sites during catalytic reactions. The specific π and σ electronic structures and the lower work functions of UNDDs probably induced by their high curvatures inevitably endow them with a higher surface energy that may be beneficial to improve the catalytic activity. The results of two probe reactions (nitrobenzene reduction and selective oxidation of 2,3,6-trimethylphenol) further demonstrate the above hypothesis about the relationship between the electronic structure and the catalytic activity. Our work provides valuable information for understanding the influence of different hybridized carbon structures and electronic properties on catalytic reactions and mechanisms.

This work was supported by "Strategic Priority Research Program" of the Chinese Academy of Sciences (Grant No. XDA09030103) and the NSFC of China (11504386). Open Access funding provided by the Max Planck Society.

Notes and references

1 (*a*) D. S. Su, S. Perathoner and G. Centi, *Chem. Rev.*, 2013, **113**, 5782; (*b*) S. Navalon, A. Dhakshinamoorthy, M. Alvaro and H. Garcia, *Chem. Rev.*, 2014, **114**, 6179.
2 (*a*) H. Watanabe, S. Asano, S.-I. Fujita, H. Yoshida and M. Arai, *ACS Catal.*, 2015, **5**, 2886; (*b*) J. Diao, H. Liu, J. Wang, Z. Feng, T. Chen, C. Miao, W. Yang and D. S. Su, *Chem. Commun.*, 2015, **51**, 3423; (*c*) K. Gong, F. Du, Z. Xia, M. Durstock and L. Dai, *Science*, 2009, **323**, 760.
3 (*a*) V. N. Mochalin, O. Shenderova, D. Ho and Y. Gogotsi, *Nat. Nanotechnol.*, 2012, **7**, 11; (*b*) A. Krueger, *J. Mater. Chem.*, 2008, **18**, 1485; (*c*) D. Pech, M. Brunet, H. Durou, P. Huang, V. Mochalin, Y. Gogotsi, P.-L. Taberna and P. Simon, *Nat. Nanotechnol.*, 2010, **5**, 651; (*d*) P. Simon and Y. Gogotsi, *Nat. Mater.*, 2008, **7**, 845–854.
4 (*a*) S. Osswald, G. Yushin, V. Mochalin, S. O. Kucheyev and Y. Gogotsi, *J. Am. Chem. Soc.*, 2006, **128**, 11635; (*b*) J.-F. Cui, X.-W. Fang and K. Schmidt-Rohr, *J. Phys. Chem. C*, 2014, **118**, 9621–9627.
5 (*a*) B. Zhong, J. Zhang, B. Li, B. Zhang, C. Dai, X. Sun, R. Wang and D. S. Su, *Phys. Chem. Chem. Phys.*, 2014, **16**, 4488; (*b*) Y. Lin, X. Pan, W. Qi, B. Zhang and D. S. Su, *J. Mater. Chem. A*, 2014, **2**, 12475; (*c*) Y. Lin and D. Su, *ACS Nano*, 2014, **8**, 7823.
6 (*a*) X. Sun, R. Wang, B. Zhang, R. Huang, X. Huang, D. S. Su, T. Chen, C. Miao and W. Yang, *ChemCatChem*, 2014, **6**, 2270; (*b*) R. Wang, X. Y. Sun, B. S. Zhang, X. Y. Sun and D. S. Su, *Chem. – Eur. J.*, 2014, **20**, 6324; (*c*) X. Liu, B. Frank, W. Zhang, T. P. Cotter, R. Schlogl and D. S. Su, *Angew. Chem., Int. Ed.*, 2011, **50**, 3318; (*d*) D. S. Su, N. Maksimova, J. J. Delgado, N. Keller, G. Mestl, M. J. Ledoux and R. Schlögl, *Catal. Today*, 2005, **102–103**, 110–114.
7 J. Zhang, D. S. Su, R. Blume, R. Schlögl, R. Wang, X. Yang and A. Gajovic, *Angew. Chem., Int. Ed.*, 2010, **49**, 8640.
8 Y. Lin, B. Li, Z. Feng, Y. A. Kim, M. Endo and D. S. Su, *ACS Catal.*, 2015, **5**, 5921.
9 J. O. Muller, D. S. Su, U. Wild and R. Schlogl, *Phys. Chem. Chem. Phys.*, 2007, **9**, 4018.
10 O. O. Mykhaylyk, Y. M. Solonin, D. N. Batchelder and R. Brydson, *J. Appl. Phys.*, 2005, **97**, 074302.
11 M. Zeiger, N. Jackel, V. N. Mochalin and V. Presse, *J. Mater. Chem. A*, 2016, **4**, 3172.
12 T. Petit, J.-C. Arnault, H. A. Girard, M. Sennour and P. Bergonzo, *Phys. Rev. B: Condens. Matter Mater. Phys.*, 2011, **84**, 233407.
13 A. S. Barnard, S. P. Russo and I. K. Snook, *Phys. Rev. B: Condens. Matter Mater. Phys.*, 2003, **68**, 073406.
14 G. C. C. Costa, J. K. McDonough, Y. Gogotsi and A. Navrotsky, *Carbon*, 2014, **69**, 490.
15 (*a*) D. S. Sutar, G. Singh and V. D. Botcha, *Appl. Phys. Lett.*, 2012, **101**, 103103; (*b*) S. H. Lim, H. I. Elim, X. Y. Gao, A. T. S. Wee, W. Ji, J. Y. Lee and J. Lin, *Phys. Rev. B: Condens. Matter Mater. Phys.*, 2006, **73**, 045402.
16 D. Holec, M. A. Hartmann, F. D. Fischer, F. G. Rammerstorfer, P. H. Mayrhofer and O. Paris, *Phys. Rev. B: Condens. Matter Mater. Phys.*, 2010, **81**, 235403.
17 M. Shiraishi and M. Ata, *Carbon*, 2001, **39**, 1913.
18 H. Ago, T. Kugler, F. Cacialli, W. R. Salaneck, M. S. P. Shaffer, A. H. Windle and R. H. Friend, *J. Phys. Chem. B*, 1999, **103**, 8116.
19 A. Siokou, F. Ravani, S. Karakalos, O. Frank, M. Kalbac and C. Galiotis, *Appl. Surf. Sci.*, 2011, **257**, 9785.
20 M. Shiraishi and M. Ata, *Mater. Res. Soc. Symp. Proc.*, 2001, **72**, 633.